Image reconstruction of concrete based on Filtered Backprojection method using ultrasonic time of flight data

Honghui Fan[1, 2*], Hongjin Zhu[1, 3], Qingbang Han[4]

[1]*School of Computer Engineering, Jiangsu University of Technology, Changzhou 213001, Jiangsu, China*

[2]*Sichuan Province Key Laboratory of Bridge non-destructive testing and engineering computing, Zigong 643000, Sichuan, China*

[3]*Key Laboratory of Cloud Computing & Intelligent Information Processing of Changzhou City, Changzhou 213001, Jiangsu, China*

[4]*College of IOT Engineering, Hohai University, Jiangsu 213022, China*

Abstract

This research aims to recognize the defect of concrete materials using an ultrasonic computed tomography imaging technique. Filtered Backprojection method was used to reconstruct concrete images in this paper. Ultrasonic time of flight data was measured to reconstruct computer tomography images. 306 data paths were obtained in total by manual scanning for one computer tomography image. We examined the effect of the interpolation data as the density of time of flight data has a considerable effect on image quality. The feasibility of concrete reconstruction system and time of flight data interpolation were examined in detail using numerical and concrete phantoms.

Keywords: Image reconstruction, Time of flight, Filtered Backprojection, Interpolation, Concrete

1 Introduction

Concrete is currently the most widely used construction material. Its huge popularity is the result of a number of well-known advantages, such as low cost, general availability, and wide applicability. Testing and quality checkup is important at different stages during the life of a structure [1, 2]. The traditional method of evaluating the quality of concrete in civil structures is to test specimens cast simultaneously for compressive, flexural, and tensile strengths; these methods have several disadvantages such as the absence of immediate result prediction [3].

Computer tomography seems to provide a better alternative for quality inspection since it provides the visual difference as reflected in the radiation attenuation profile, radiation attenuation distribution, detail position and detail dimension [4, 5]. Ultrasonic time of flight (TOF) computed tomography was applied to evaluate wooden pillars quality by Tomikawa et al [6]. In the recent research reports, Filtered Backprojection (FBP) algorithm was used for image reconstruction [7-9]. The FBP algorithm was modified to reconstruct computed tomography images from incomplete TOF profiles of wood by Yanagida [10]. FBP algorithm has been extended to fan beam data acquisition geometry in some report [11-13], and has been widely used in industrial computer tomography [14].

In ultrasonic TOF computer tomography, the spatial distribution of sound velocity is estimated [15].

Ultrasonic TOF data testing of concrete is based on ultrasonic velocity in concrete method to provide information on the uniformity of concrete, cavities, cracks and defects [16-18]. The date of TOF in concrete depends on its density and its elastic properties, which in turn are related to the quality and the compressive strength of the concrete. It is therefore possible to obtain information about the properties of components by ultrasonic velocity [19].

FPB algorithm is an image reconstruction method for ultrasonic TOF computer tomography. It was modified to reconstruct computer tomography images from the incomplete time of flight profiles of wood by Fan and of concrete by Suryono et al [20, 21]. Although the quality of the object can be determined, it is difficult to accurately find the position of the holes in reconstruction images [22, 23]. In this paper, we proposed an approach to concrete inspection by ultrasonic TOF computer tomography on the basis of the FBP algorithm. Furthermore, the interpolation of TOF data was applied to enhance image quality in FBP imaging process. The effects of image quality and the number of interpolations in the TOF data were examined in detail with concrete phantom.

2 Image reconstruction using FBP algorithm

FBP algorithm for parallel beam projection data with and without attenuation has been well established [24]. Without attenuation, the FBP algorithm has been

---

Fan Honghui, Zhu Hongjin, Han Qingbang

extended to fan-beam data acquisition geometry, and has been widely used in computer tomography.

The FBP turns to Fourier theory to approach the problem of finding the linear attenuation coefficient at various points in the cross-section of an object [25]. A fundamental result linking Fourier transform to cross-sectional images of an object is the Fourier Slice Theorem [26], and this paper only concerns parallel beam projection data. The Fourier Slice Theorem for the parallel beam projection data is given here. The same justifications can be made for fan beam and cone beam projection data.

When the data I_o obtained from the observation is expressed as a function by the line integral for route s physical weight distribution $f(x, y)$ of the measurement section.

$$I_o = \int_s f(x,y)ds. \qquad (1)$$

The arrangement is shown in Figure 1, $P(r, \theta)$ is the projection data obtained at position r, and observed from direction θ. r-s coordinate system that is rotated by an angle θ from the x=y coordinate system.

$P(r, \theta)$ could be represented by the Equation (2). Here, δ is delta function of Dirac, and the Equation (2) is called Radon transform.

$$
\begin{aligned}
P(r,\theta) &= \int_{-\infty}^{\infty} f(r\cos\theta - s\sin\theta, r\sin\theta + s\cos\theta) \\
&= \int_{-\infty}^{\infty}\int_{-\infty}^{\infty} f(x,y)\delta(x\cos\theta + y\sin\theta - r)dxdy
\end{aligned}
\qquad (2)
$$

$$F(\mu,\nu) = \int_{-\infty}^{\infty}\int_{-\infty}^{\infty} f(x,y)\exp\{-j2\pi(\mu x + \nu y)\}dxdy, \qquad (3)$$

$$F(\rho\cos\theta,\rho\sin\theta) = \int_{-\infty}^{\infty}\int_{-\infty}^{\infty} f(x,y)\exp\{-j2\pi\rho(x\cos\theta + y\sin\theta)\}dxdy, \qquad (4)$$

$$
\begin{aligned}
F(\rho\cos\theta, \rho\sin\theta) &= \int_{-\infty}^{\infty}\left[\int_{-\infty}^{\infty} f(r\cos\theta - s\sin\theta, r\sin\theta + s\cos\theta)ds\right]\exp\{-j2\pi\rho r)dr \\
&= \int_{-\infty}^{\infty} p(r,\theta)\exp\{-j2\pi\rho r)dr
\end{aligned}
\qquad (5)
$$

$$f(x,y) = \int_{-\infty}^{\infty}\int_{-\infty}^{\infty} F(\mu,\nu)\exp\{j2\pi(\mu x + \nu y)\}dxdy. \qquad (6)$$

Equation (5) indicates that Fourier transforms of projection data $P(r, \theta)$ from the angle θ is identical to the cross-section cut at angle θ spectra of the two-dimensional Fourier transform of a physical quantity distribution $f(x, y)$. Thus, two dimensional Fourier spectrum is obtained by collecting the projection data from all directions, and restored physical quantity distribution $f(x, y)$ from a set of projection data $P(r, \theta)$ by working the inverse operator. Equation (6) expresses the method of conversion Equation (5) to two dimensional inverse Fourier transform.
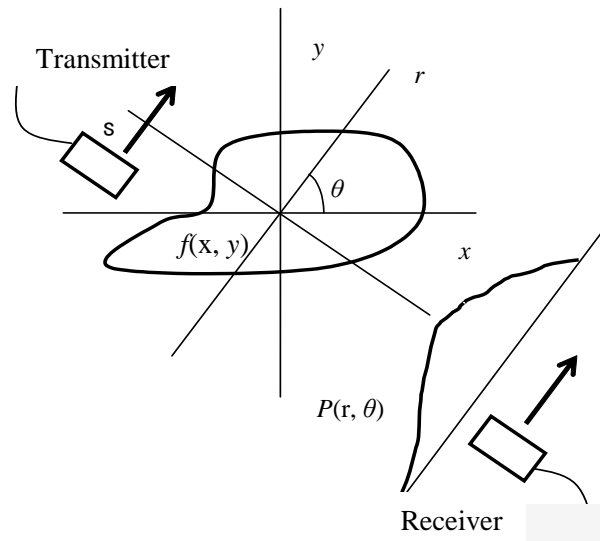

FIGURE 1 Object $f(x, y)$ and its projection $P(r, \theta)$

Based on Equation (2), $f(x, y)$ from $P(r, \theta)$ could be calculated easily by using two-dimensional Fourier transform and Equation (3).

Here, $\mu=\rho\cos\theta$, $\nu=\rho\sin\theta$ make a polar coordinate conversion. And using Equation (2), Equation (5) could get

However, because the calculation amount is large, the FBP method is often used in this process. Polar coordinates transform the Equation (6) by using the symmetry of the Fourier transform. Equation (7) is composed as follows.

$$f(x,y) = \int_{-\infty}^{\infty}\left[\int_{-\infty}^{\infty} G(\rho)|\rho|\exp(j2\pi\rho r)d\rho\right]d\theta. \qquad (7)$$

Here,

$$G(\rho) = \int_{-\infty}^{\infty} p(r,\theta)\exp(-j2\pi\rho r)dr \,. \qquad (8)$$

The system is intended to apply to the contact type transmission time computer tomography image reproduction principle using the FBP method. Physical quantity to be measured in our system since the propagation time, the projection data are represented as follows.

$$TOF(i,j) = \int_s \frac{1}{c(x,y)} ds \,. \qquad (9)$$

Here, (i, j) is measurement point number, TOF (i, j) is time of flight data when measurement point i be used as transmission point, and measurement point j be used as reception point. In addition, s is the shortest path of time flight, $c(x, y)$ shows a sound speed distribution in the measured cross-section.

In Equation (1), I_o replaced by TOF (i, j), $f(x, y)$ replaced by $1/c(x, y)$, TOF could be considered as a projection. Therefore, the image obtained by the reconstruction is distributed of the inverse of the sound velocity c (slowness).

In the Equation (10) above, the terms inside the square brackets (the operation indicated by the inner integral) represent a filtering operation and evaluate the filtered projections. The operation being performed by the outer integral evaluates the back projections, which basically represents a smearing of the filtered projections back onto the object and then finding the mean over all the angles.

Given that n rays pass through a measuring section, li is the length of ray i (distance between transmission and reception transducer), t_i is the time that ray travels along li. From Randon transform,

$$\tau_i = \int_{L_i} \frac{1}{V_j(x,y)} dl = \int_{L_i} f_j(x,y)dl \,, \qquad (10)$$

where $V_j(x, y)$ is the velocity of cell j, $f_j(x, y)$ is the slowness of cell j. It is assumed that the cell is small enough, so $f_j(x, y)$ of each cell can be considered as constant. Equation (11) can be written as progression form,

$$\varsigma_j = \sum_{j-1}^{m} a_{ij} f_j \,, \qquad (11)$$

where a_{ij} is the length of ray i in cell j. In view of mathematics Equation (12) is a linear equation group.

$$\begin{cases} \tau_1 = a_{11}f_1 + a_{12}f_2 + \cdots + a_{1m}f_m \\ \tau_2 = a_{21}f_1 + a_{22}f_2 + \cdots + a_{2m}f_m \\ \vdots \\ \tau_n = a_{n1}f_1 + a_{n2}f_2 + \cdots + a_{nm}f_m \end{cases}. \qquad (12)$$

3 Experimental Methods

3.1 EXPERIMENTAL SYSTEM

The experimental system was shown in Figure 2. A couple of bolt-clamped Langevin-type transducers (BLT) of 68 kHz centre frequency were used as an ultrasound transmitter and a receiver.

The 36 measurement points were placed on the circumference of the test sample and labelled 0 to 35. Every measurement point transmits and receives ultrasonic signals in our system.

36 measuring points were placed 10 degrees (θ_c=10º) apart on the circumference of the test sample and labelled with numbers from 0 to 35. The burst wave was transmitted from the l-th point and received at the m-th point with a gap number n, that is, $m=(l+n)_{\text{mod36}}$. When gap angle θ_c=10º, the gap of numbers between the transmitter and receiver, n, was kept for $\theta_c/10$=1 such as (transmitter 0, receiver 1), (1, 2), …(l, m),…(35, 0(=(35+1)_{\text{mod36}})).

TOF for a gap number n was described as $t_l^{(n)}$, where l is the number of measuring point. TOF of gap angle θ_c=10º can be described as

$$t_l^{(n)} = t_l^{(i)} \quad \left(l = 0 \cdots 35 \right). \qquad (13)$$
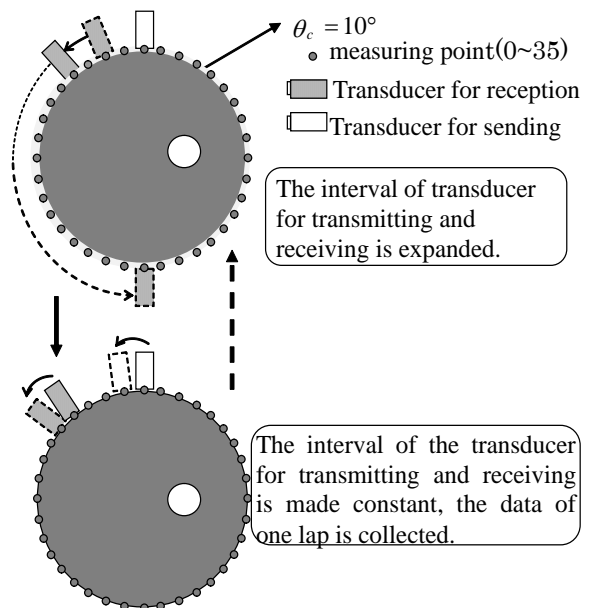

FIGURE 2 Measurement procedures

74

When wave data were received, there were some noises of low-frequency and high-frequency. To remove the noises from the measurement data, a band pass filter of 10–100 kHz was used for all TOF data. After the filtering, the amplitudes of the wave data were calculated. To avoid error detection by high-frequency noise, 20% of the maximum amplitude value of each wave data was used as threshold levels for TOF detection (Figure 3).
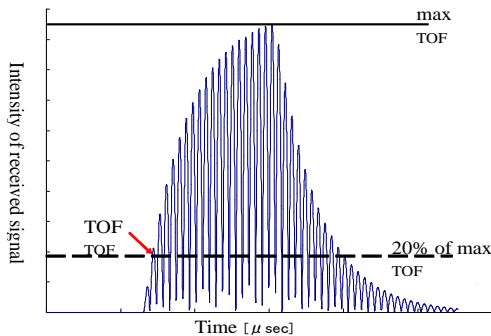

FIGURE 3 The TOF determination

3.2 TOF DATA INTERPOLATION

The wavelength of ultrasound of 68 kHz was about 20 mm. 36 measurement points were placed on the circumference. The distance of the interval was about 17mm. All measurement paths were 306. It takes about two hours to obtain 306 TOF for one computer tomography image. So, the number of data that can be measured is thought that 306 were near the upper bound timely and spatially. However, the 306 data was not enough to obtain a clear computer tomography image. To raise the pixel level, angle interpolation for fan beam and distance interpolation for parallel beam were used in the imaging process. The TOF data were obtained measured with the fan - beam geometry of non-equal and coarse intervals. The obtained TOF profiles are converted into the small and regularly-interval data by the spline interpolation.

In the case of θ_c=10°, the measurement path, such as (0, 1), (0, 3), (0, 5) … (0,35) was interpolated, and TOF data with a denser fan beam geometry was obtained. So one measurement point would be passed by more fan-beam, such as (transmitter 0, receiver 1), (0, 2), (0, 3) … (0, 34), (0, 35). The number of paths was 35 with one measurement point, the TOF data number became 612 {= (number of measurement point 36 × measurement path from one measurement point 35 - duplicate path of diameter route 36) ÷exchange 2} after angle interpolation.

The second step interpolation was used for obtaining the parallel beam with equal intervals of measurement path distance. After angle interpolation, such as (0, 1), (35, 2), (34, 3) … (19, 18), the number of measurement path with same horizontal was 19. Using distance interpolation we could get 39 (=19 × 2+1) path for one horizontal parallel beam, so total interpolation TOF data of 1404 (=39 × 36) paths were obtained. After these

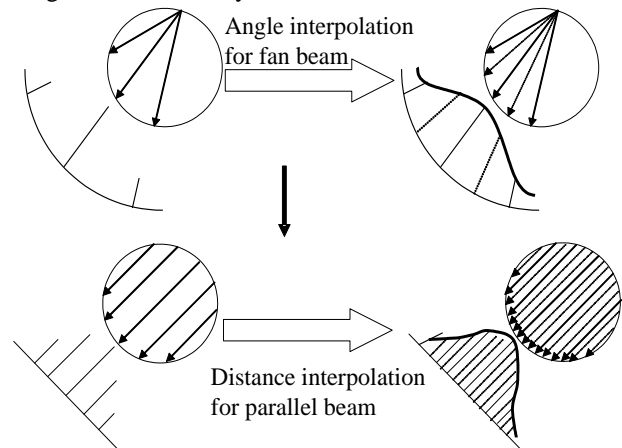interpolations, one 64 × 64 pixel computer tomography image could be clearly reconstructed.

FIGURE 4 TOF data interpolation by fan beam geometry and parallel beam geometry

The process of reconstruction image based on FBP method in our system is shown in Figure 5. The position of measurement points and shape data were first calculated according to coordinates of measurement points and measurement object. According to the interval of transducer for sending and reception, all ultrasonic velocity data were made up of 9 groups. Interpolation TOF data was got using fan beam and parallel beam geometry under measurement TOF beam profile, and pixel value was designated on that wave path. A computer tomography image could be reconstructed based on FBP algorithm.
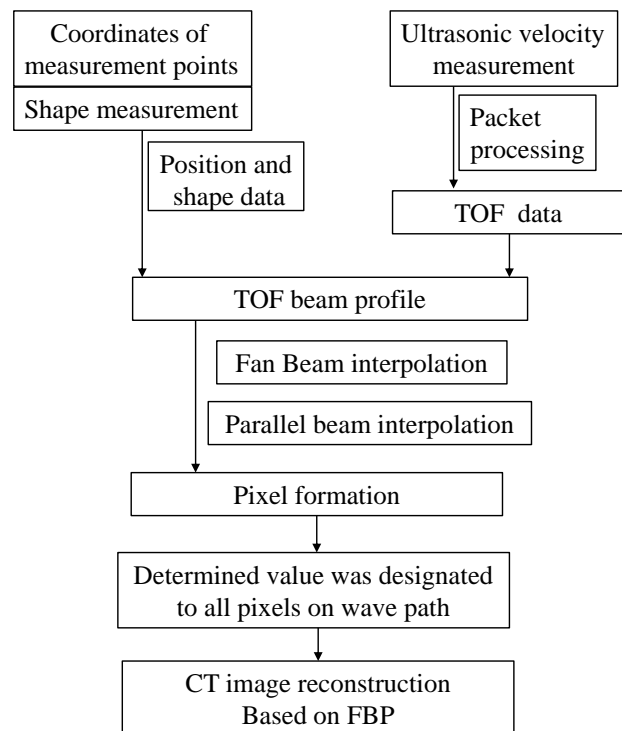

FIGURE 5 Flowchart for reconstruction image based on FBP

4 Results

4.1 NUMERIAL PHANTOM

A numerical phantom containing a circle shaped defect was assumed which was composed of 64 x 64 square pixels. The acoustic velocities were 5000 m/s for normal part, the acoustic velocities 2500 m/s for defect part. Parameters of numerical concrete phantom were shown in Table 1.

TABLE 1 Parameters of concrete

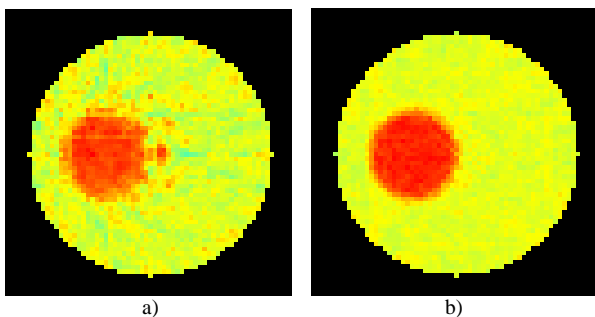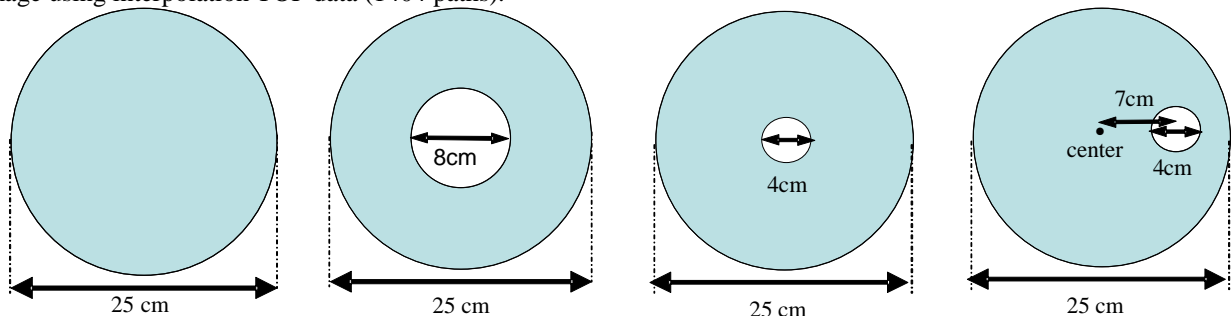| Property	Normal part 5000 [m/s]	Defect part 2500 [m/s]
Poisson's ratio	0.3	0.3
Young's modulus [N/mm2]	1.075×1010	2.688×109
Density [kg/m3]	430	430

a)　　　　　　　　b)

FIGURE 6 Reconstruction images of numerical phantom

The reconstruction images based on FBP method are shown in Figure 6. Figure 6a is the reconstruction image which uses 306 TOF data, Figure 6b is the reconstruction image using interpolation TOF data (1404 paths).

From the reconstructed images which without interpolation, some artefacts were observed in the images and no clear defects were observed. When angle and distance interpolation TOF data was used, the better-quality computer tomography images could be reconstructed.

4.2 CONCRET PHANTOM

Four concrete test specimens (A test concrete phantom, B test concrete phantom, C test concrete phantom and D test concrete phantom) were produced for the verification of the proposed experimental system. The test specimens were composed of mortar and Styrofoam. A test concrete phantom was consisted entirely of mortar, and was without defect. B, C and D test concrete phantoms were consisted entirely of mortar and polystyrene foam. As shown in Figure 7, B and C test concrete phantoms had a defect which was set in the centre, and the diameter of the defect was 8 cm and 4 cm respectively. All of the test specimen diameters were 25 cm.

The images in Figure 8 were the reconstruction results of the four test concrete phantoms. Test concrete phantoms could be reconstructed based on FBP algorithm. The different defects in the three test concrete phantoms could be found in the reconstructed images. The defect position and size of B, C and D test concrete phantoms were observed, but it was possible that some artefacts were recognized. The results demonstrated the effectiveness of the proposed algorithm.
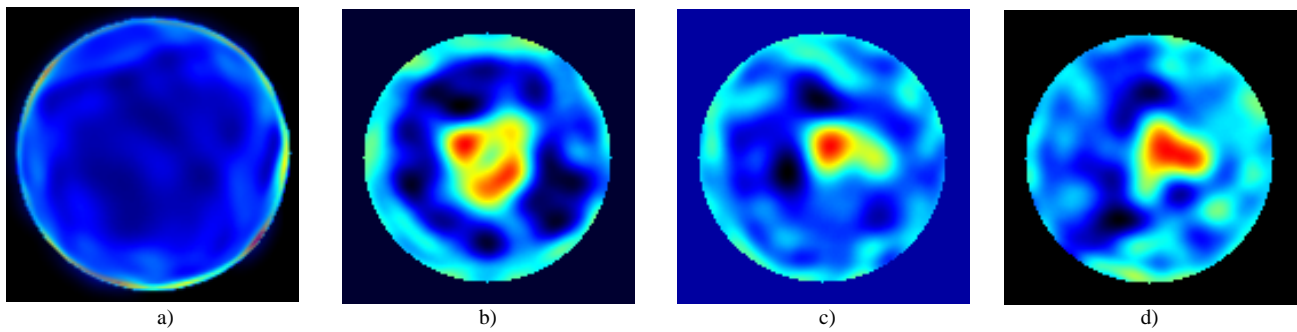

A　　　　　　B　　　　　　C　　　　　　D

FIGURE 7 Inspection object

a)   b)   c)   d)

FIGURE 8 Reconstruction results of the four test concrete phantoms

5 Discussions

When the FBP method was used for the ultrasonic computer tomography of concrete, 306 TOF data were not sufficient to obtain clear images. By applying the FBP method to ultrasonic computer tomography, we should obtain more TOF data or use an interpolation in the imaging process. Defects with diameters ranging from 4cm to 8cm were recognized by visual observation. However, the defects could not be found clearly in the reconstructed images of the concrete phantom. By comparing the reconstruction images with numerical phantom and concrete phantom, we concluded that visually, the defect was clearly reconstructed in the numerical phantom, and the defects could not be found clearly in the reconstructed images of concrete phantoms. The reason was considered that the sound propagation path was a straight line and it intends to reconstruct the concrete section image in proportion to the distribution of the equivalent sound velocity. The anisotropic property of concrete and Volatility of ultrasonic were not considered in our system.

References

[1] Mehta P K 2002 *Concrete International* **24**(7) 23-8
[2] Meyer C 2009 *Cement and Concrete Composites* **31** 601-5
[3] Maiti S C, Agarwal K 2009 *The Indian concrete journal* September 20-7
[4] Chauhan M S 2013 *International Research of Sustainable Science and Engineering* **1**(1) 1-3
[5] Chai H K, Momoki S, Kobayashi Y, Aggelis D G, Shiotani T 2011 *NDT and E International* **44** 206-15
[6] Tomikawa Y, Iwase Y, Arita K, Yamada H 1986 *IEEE Trans. Ultrason.Ferroelectr. Freq. Control* **33** 354
[7] Jiangsheng Y, Gengsheng L, Zhengrong L 2005 *Inverse Problems* **21**(5) 1801
[8] Joshua D E, David G P, Bruce R W, Joseph O S, Jeffrey F W 2011 *Medical Physics* **38**(3) 1444-58
[9] James B, Susu Y, Justin Roper, William G, Fangfang Y 2014 *Medical Physics* **41**(1) 010701
[10] Hirotaka Y, Yasutaka T, Kwang M K, Jun J J 2007 *Japanese Journal of Applied Physics* **46**(8) 5321-5
[11] Xiaochuan P, Dan X, Yu Z, Lifeng Y 2004 *Physics in Medicine and Biology* **49**(18) 4349-69
[12] Jongduk B, Norbert J P 2010 *Medical Physics* **37**(5) 2074-81
[13] Adam W, Frederic N 2008 *Physics in Medicine and Biology* **53**(10) 2471-93
[14] Suryono, Kusminarto, Bayu S, Aris S 2011 *International Journal of Civil and Environmental Engineering* **11**(5) 17-22
[15] Honghui F, Hirotaka Y, Yasutaka T, Shuqiang G, Tadashi S, Tasuhisa T 2010 *Japanese Journal of Applied Physics* **49** 07HC12
[16] Wunderlich C, Niederleithinger E 2013 *Nondestructive Testing of Materials and Structures* **6** 227-32
[17] Lee K M, Kim Y H, Bae D B 2004 *Cement and Concrete Research* **34** 631-40
[18] Mullapudi T R, Di G, Ashraf A 2013 *Magazine of Concrete Research* **65**(18) 1081-91
[19] Adam F, Jirl J, Igor P 2012 R*adio Engineering* **21**(1) 533-44
[20] Honghui F, Hongjin Zang, Yao W 2013 *Review on Computers and Software* **8**(1) 17-20
[21] Alwin S, Antariksa S, Purnama S 2013 *Journal of Basic and Applied Scientific Research* **3**(8) 418-22
[22] Schickert M 2005 *Materials and Structures* **38** 807-15
[23] Yanli C 2010 I*nternational Forum on Information Technology and Applications* **1** 392-6
[24] Hongli S, Shuqian L 2013 *Bio Medical Engineering Online*: http://www.biomedical-engineering-online.com/content/12/1/50
[25] Wang K, Anastasio M A 2012 *Physics in Medicine and Biology* **57**(23) N493
[26] Chiou S F, Shih S L 1998 *Image and Vision Computing* **16**(9-10) 689-701

Authors

Honghui Fan, born in October, 1980, Shandong Province

Current position, grades: School of Computer Engineering, Jiangsu University of Technology, Changzhou, Jiangsu, China, Associate professor.
University studies: Systems and Information Engineering
Publications: 11 publications
Experience: He has a M.Sc. And Ph.D. from the Yamgata University of Japan in 2008 and 2011, respectively. He is a member of China Computer Federation. In 2011 he joined Jiangsu University of Technology. His research interests include ultrasound imaging, image restoration, digital image, and signal processing in biomedical engineering.

Hongjin Zhu, born in May, 1981, Jilin Province

Current position, grades: School of Computer Engineering, Jiangsu University of Technology, Changzhou, Jiangsu, China, Lecturer.
University studies: Systems and Information Engineering
Publications: 10publications
Experience: She has an M.Sc. And Ph.D. from the Yamgata University of Japan in 2007 and 2010, respectively. She was employed as a special researcher in the Department of Engineering, Yamagata University of Japan in 2010. In 2011 she joined Jiangsu University of Technology. Her research interests include image processing, computer vision, pattern recognition and evolutionary computation.

Qingbang Han

Current position, grades: College of IOT Engineering, Hohai University, Jiangsu, China, Professor.
University studies: Acoustic and information processing technology
Publications: 25 publications
Experience: His research interests include signal processing, NDT, Acoustic wave propagation characteristics and Power ultrasonic.